Chemistry–A European Journal
Research Article
doi.org/10.1002/chem.202301205
Chemistry Europe
European Chemical Societies Publishing
www.chemeurj.org

Special Collection

The Best of Both Worlds: Combining the Power of MICs and WCAs To Generate Stable and Crystalline Cr^{I}-Tetracarbonyl Complexes with π-Accepting Ligands

Tobias Bens,[a] Robert R. M. Walter,[a] Julia Beerhues,[a, b] Manuel Schmitt,[c] Ingo Krossing,[c] and Biprajit Sarkar*[a]

Abstract: Here we present stable and crystalline chromium(I) tetracarbonyl complexes with pyridyl-MIC (MIC = mesoionic carbene) ligands and weakly coordinating anions (WCA = $[Al(OR^F)_4]^-$, $R^F = C(CF_3)_3$ and $BAr^F = [B(Ar^F)_4]^-$, $Ar^F = 3,5\text{-}(CF_3)_2C_6H_3$). The complexes were fully characterized via crystallographic, spectroscopic and theoretical methods. The influence of counter anions on the IR and EPR spectroscopic properties of the Cr^{I} complexes was investigated, and the electronic innocence versus non-innocence of WCAs was probed. These are the first examples of stable and crystalline $[Cr(CO)_4]^+$ complexes with a chelating π−accepting ligand, and the data presented here are of relevance for both the photochemical and the electrochemical properties of these classes of compounds.

Introduction

Group 6 tetracarbonyl complexes of the type $[M(CO)_4(L)]$ (M = Cr, Mo, W; L = chelating π−accepting ligands)[1–11] have received increasing attention due to their intriguing physical and chemical properties.[7,12] They are attractive candidates for electrochemical and photophysical bond activation, which makes them suitable compounds for electrochemical CO_2 reduction[4,6–8,10] and photoredox catalysis.[9]

In the last 50 years, great efforts have been made to study the photophysical/photochemical[2,3,11,13,14] and electrochemical[1,4,6,8,10,11,15,16–20] properties of such systems. Photoexcitation of carbonyl complexes of zero-valent group 6 metals with chelating π−accepting ligands can sometimes lead to emissive states,[21,22] but CO dissociation is often the main consequence of light excitation in these molecules.[1,3,22,23,24] The MLCT excited states are indirectly linked to the oxidized and the reduced forms of the ground state of such molecules. Thus, the photochemistry and the redox chemistry of these systems are often studied hand in hand. In this context, it was observed early on in the research of such compounds that the oxidation step of $[M(CO_4)L]$ with π−accepting ligands, as investigated by cyclic voltammetry, is often irreversible.[11,16,18–20] Only in very few cases a reversible oxidation has been observed, albeit only at low temperatures.[25] This irreversibility is due to the kinetic lability and uncompensated electron deficiency of the central metal atom, resulting in decreased π−backdonation from the metal center to the CO ligand and consequently weakening of the M–CO bond.[16–20] Thus, attempts to isolate, crystallize and thoroughly characterize such oxidized species with π−accepting chelating ligands have never been successful.

Some of us have recently shown that pyridyl-mesoionic carbene (MIC) chelating ligands (Scheme 1) are a privileged class of ligands that retain a similar π−accepting property to 2,2′-bipyridine (bpy), while at the same time incorporating the excellent σ−donor properties of a MIC.[26] Investigations with Re^{I} compounds as well as with group 6 compounds[1–3] clearly demonstrated both the good π−accepting and σ−donor properties of this ligand class.[27]

Recently, Krossing and co-workers developed a synthetic strategy to access the homoleptic 17 VE $[M(CO)_6]^+$ (M = Cr, Mo, W) complexes with weakly coordinating anions ($WCA^- = [Al(OR^F)_4]^-$ with $R^F = C(CF_3)_3$) to overcome CO dissociation, substitution and dimerization of the so-called (super-)electrophiles.[28] In the following, we show that by combining WCA or BAr^F (= tetrakis(3,5-bis(trifluoromethyl)-phenyl)borate) with our pyridyl-MIC ligands (C–C = pyridyl-4-triazolylidene[26] and C-N = pyridyl-1-triazolylidene)[1] it is possible to isolate cationic $[Cr(CO)_4$(pyridyl-MIC)](WCA) complexes with

[a] T. Bens, R. R. M. Walter, Dr. J. Beerhues, Prof. Dr. B. Sarkar
Institut für Anorganische Chemie
Universität Stuttgart
Pfaffenwaldring 55, 70569 Stuttgart (Germany)
E-mail: biprajit.sarkar@iac.uni-stuttgart.de
Homepage: http://www.iac.uni-stuttgart.de/en/research/aksarkar/
[b] Dr. J. Beerhues
Current Address: Institute of Chemical Research of Catalonia (ICIQ)
Barcelona Institute of Science and Technology (BIST)
Av. Paisos Catalans 16, 43007 Tarragona (Spain)
[c] M. Schmitt, Prof. Dr. I. Krossing
Institut für Anorganische und Freiburger Materialforschungszentrum (FMF)
Universität Freiburg
Albertstr. 21, 79104 Freiburg (Germany)

Supporting information for this article is available on the WWW under https://doi.org/10.1002/chem.202301205

Special Collection This manuscript is part of a special collection on 3rd International Conference on Organometallics and Catalysis (ICOC-2023).

Research Article
doi.org/10.1002/chem.202301205
Chemistry Europe
European Chemical Societies Publishing

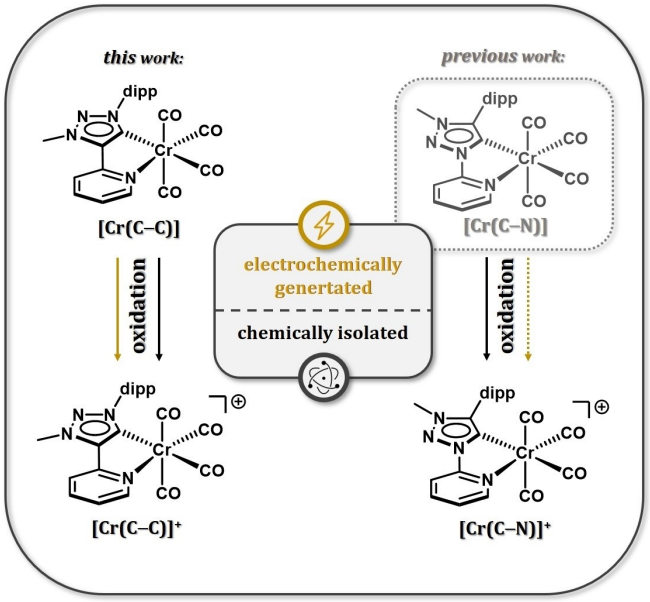

Scheme 1. Chemical (black) and electrochemical (yellow) oxidation of [Cr(C–C)] and [Cr(C–N)]. The neutral complex [Cr(C–N)] (top, right) was reported previously.[1]

π−accepting ligands, similar to those of bpy, as stable and crystalline material (Scheme 1).[26]

Results and Discussions

The 18 VE complex [Cr(C–C)] was synthesized according to a previously described protocol in our group with irradiation of $[Cr(CO)_6]$ for 2 h in THF and subsequent addition of the corresponding triazolium salt $[H(C–C)]BF_4$ in the presence of a base (NEt_3). Crystallization from a concentrated solution of [Cr(C–C)] in CH_2Cl_2 and *n*-hexane, yielded 64% red crystals suitable for X-ray diffraction (Figure 1). All metal-ligand as well as intra-ligand bond lengths are in the expected range and fit nicely with the previously reported pyridyl-MIC [Cr(C–N)] complex (Table 1, Tables S1 and S2 in Supporting Information).[1]

The cyclic voltammogram of [Cr(C–C)] versus FcH/FcH^+ at ambient temperatures shows a reversible oxidation at −0.21 V and a reversible reduction at −2.26 V (Figure 2), followed by an irreversible second reduction at −2.80 V. These data are similar but slightly cathodically shifted compared to what was previously reported for [Cr(C–N)] (Table S4).

As the oxidation potential of Ag^+ in CH_2Cl_2 is +0.65 V versus FcH/FcH^+,[29] silver salts should in principle be able to oxidize both [Cr(C–C)] (−0.21 V) and [Cr(C-N)] (+0.17 V) complexes. However, the addition of $AgPF_6$ to [Cr(C–C)] or [Cr(C-N)] in non-coordinating CH_2Cl_2 resulted in an immediate gas evolution, even at lower temperatures of −40 °C. This observation is most likely related to the release of CO gas from the complexes on using the aforementioned silver salt, potentially

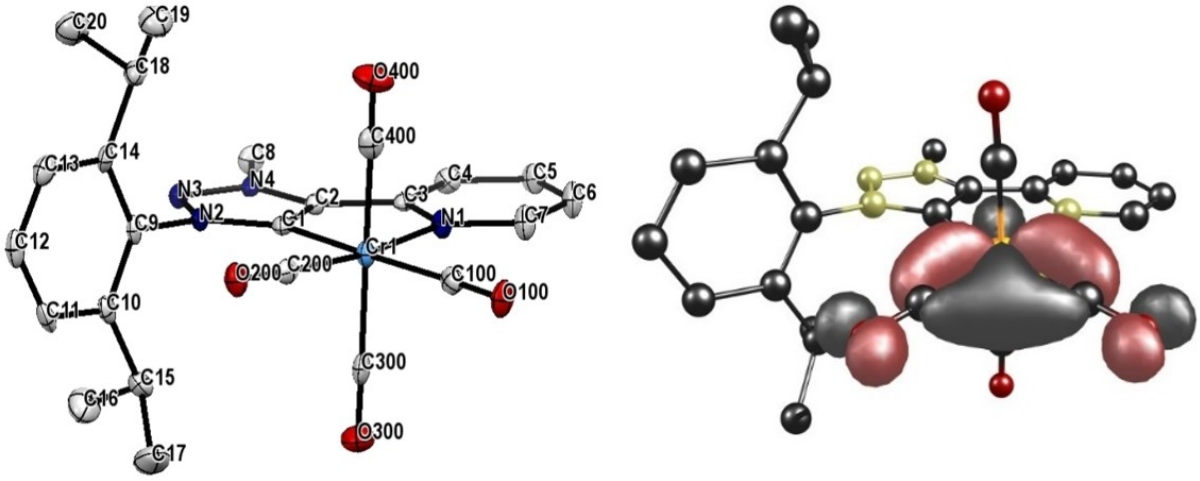

Figure 1. ORTEP representation (left) and HOMO orbital (right, iso value = 0.052, B3LYP/D3/def2-TZVP) of [Cr(C–C)] (hydrogen atoms are omitted for clarity). Ellipsoids are drawn with 50% probability.

Table 1. Selected bond lengths of [Cr(C–C)] and [Cr(C–N)] in Å.

	[Cr(C–C)]	[Cr(C–C)](BAr^F)	[Cr(C–N)][1]	[Cr(C–N)](WCA)
Cr-C1	2.049(3)	2.040(7)	2.065(2)	2.063(7)
Cr-N1	2.163(3)	2.139(6)	2.147(2)	2.118(6)
Cr-C100	1.851(3)	1.930(9)	1.855(2)	1.951(8)
Cr-C200	1.827(4)	1.925(1)	1.847(2)	1.915(9)
Cr-C300	1.906(4)	1.877(9)	1.894(2)	1.930(8)
Cr-C400	1.895(4)	1.906(1)	1.903(2)	1.898(9)

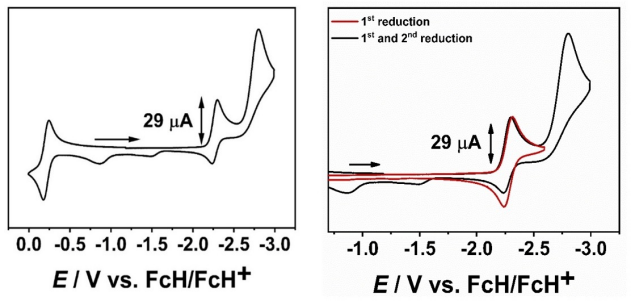

Figure 2. Cyclic voltammograms of [Cr(C–C)] in CH_3CN and 0.1 M Bu_4NPF_6 with a scan rate of 100 mV s^{-1}.

with concomitant coordination of $[PF_6]^-$. Therefore, we changed our strategy for the isolation of $[Cr(C–C)]^+$ and $[Cr(C–N)]^+$ using a synthetic protocol involving oxidizing agents based on WCAs ($Ag[WCA]$[30] and $Fc[BAr^F]$[31]).

Under exclusion of light, the chromium carbonyl complexes were dissolved in CH_2Cl_2 and the corresponding oxidizing agent was added at room temperature, resulting in an immediate color change from red to yellow. After three hours, the reaction mixture was filtered and layered with *n*-hexane at −40 °C, which ultimately yielded 87% crystalline material of $[Cr(C–C)](BAr^F)$ and 89% of [Cr(C-N)](WCA) suitable for single-crystal X-ray diffraction (Figure 3).

A comparison of the bond lengths for the neutral and oxidized complexes shows some interesting trends. The intra-ligand bond lengths within the pyridyl-MIC ligands change only slightly on moving from the neutral to the oxidized complexes. On the contrary, the metal-ligand bond distances are strongly affected on oxidation (Table 1, Tables S1 and S2). Substantial bond elongation is observed for the Cr–CO bonds in the oxidized complexes in the equatorial plane. These results agree with the fact that the HOMO of the neutral complexes is composed of a *d*-orbital that is in the equatorial plane and the π−type orbitals from the two CO ligands in that plane (Figure 1, right). Removal of electron density from that orbital will have the strongest effects on the metal ligand bond lengths that are in the equatorial plane. In keeping with the elongated Cr–CO bond distances in the equatorial plane, the corresponding CO bond lengths in that plane decrease. For $[Cr(C–C)](BAr^F)$ weak cation-anion interactions are observed between a C–F group of BAr^F and an axial CO ligand (Figure S6). The C400-F and O400-F distances are 2.951 and 2.783 Å respectively, and are smaller than the sum of the van der Waals radii of the respective atoms. No such interactions were detected for the complex [Cr-(C–N)](WCA).

In contrast to the Cr–CO bond distances, the Cr–C1 and Cr–N1 bonds to the pyridyl-MIC ligand become stronger upon oxidation. This fact is likely related to the excellent σ−donor properties of the pyridyl-MIC ligands. All these data clearly support a predominantly chromium centered oxidation in these complexes.

IR-spectroelectrochemistry (SEC) on the complex was performed in the presence of Bu_4NPF_6 as a supporting electrolyte, (Figure 4 and Figure S11) and the results are in good agreement with our theoretical B3LYP/D3/def2-TZVP calculations (Figure S10 and S12). The average shift of around 130 cm^{-1} for the CO stretching frequencies (Table 2) upon one-electron oxidation fits nicely with a Cr-centered oxidation in this complex.

Apart from the large shift of the CO bands upon one-electron oxidation, the IR data also display an effect of the counter anion on the position of the bands. Thus, the CO bands with a WCA display a slight blue shift compared to the ones with $[PF_6]^-$ as anion (see section 5.2 and 5.3 of Supporting Information).

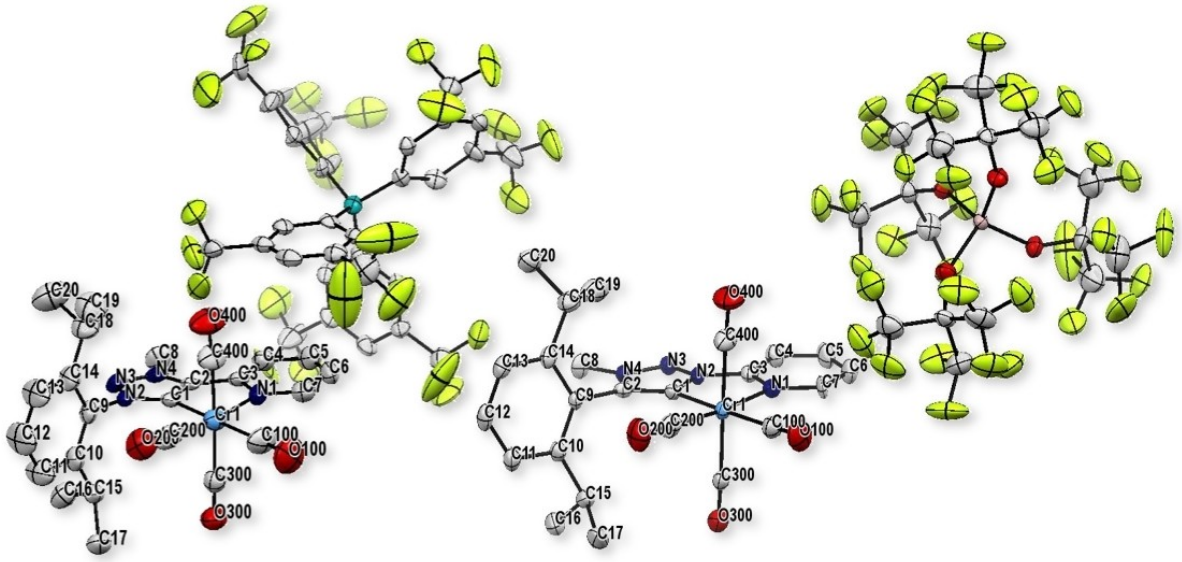

Figure 3. ORTEP representation of $[Cr(C–C)](BAr^F)$ (left) and [Cr(C-N)](WCA) (right). Hydrogen atoms are omitted for clarity. Ellipsoids were drawn with 50% probability.

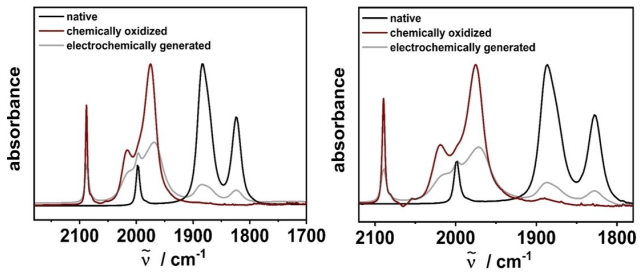

Figure 4. Left: [Cr(C–C)] (black), electrochemically generated $[Cr(C–C)]^+$ (grey) in CH_3CN/0.1 M Bu_4NPF_6 (Au WE) and [Cr(C–C)](BAr^F) in CH_2Cl_2 (red). Right: [Cr(C–N)] (black), electrochemically generated (Au WE) $[Cr(C–N)]^+$ (grey) in CH_3CN/0.1 M Bu_4NPF_6 and [Cr(C–N)](WCA) in CH_2Cl_2 (red). The Y-axis is not normalized.

Further insights into the electronic structures of the native and the oxidized complexes were obtained via UV/vis/NIR-SEC in combination with TD-DFT calculations at B3LYP/D3/def2-TZVP level. Even though results from TD-DFT calculations may not always be very accurate, they can be used to get a first insight into such transitions. Both complexes show bands between 300–500 nm (see Supporting Information, section 7). These transitions occur from the HOMO-1 and HOMO-2 orbitals, which have contributions from both Cr and CO, to orbitals that are predominantly centered on the pyridyl-MIC ligands. Such transitions can thus be assigned as MLCT with a small LLCT contribution. These results are in good agreement with previous reports on $[Cr(bpy)(CO)_4]$.[14] Depopulation of the metal centered Cr(d_{xz}) orbitals lead to weakening of the Cr–C bond and consequently rapid photodissociation from the ^{1}MLCT.[23] In the oxidized form, the MLCTs are slightly blue-shifted and show a strong contribution from the pyridyl-MIC ligand instead of CO ligands. These results indirectly indicate that the electron-deficiency of the oxidized metal-center, which results in a decreased $\pi-$backdonation, is compensated by the strongly $\sigma-$donating pyridyl-MIC ligands.

To gain a detailed insight into the electronic structure, the one-electron oxidized 17 VE complexes were further investigated by EPR-spectroscopy and compared with the electrochemically generated species (Figure 5). The slightly stronger interaction of the $[BArF]^-$ anion with the cationic metal complex

Table 2. CO stretching frequencies of [Cr(C–C)], [Cr(C–N)], [Cr(C–C)](BAr^F) and Cr(C–N)](WCA) in CH_2Cl_2.

	$\tilde{\nu}$(CO)/cm^{-1}				$\tilde{\nu}_{average}$(CO)/cm^{-1}
[Cr(C–C)]	1998	1882	1873 (sh)	1822	1894
[Cr(C–N)][1]	1998	1890	1878 (sh)	1830	1899
[Cr(C–C)](BAr^F)	2087	2015	1992 (sh)	1975	2017
[Cr(C–N)](WCA)	2089	2019	1995 (sh)	1975	2020

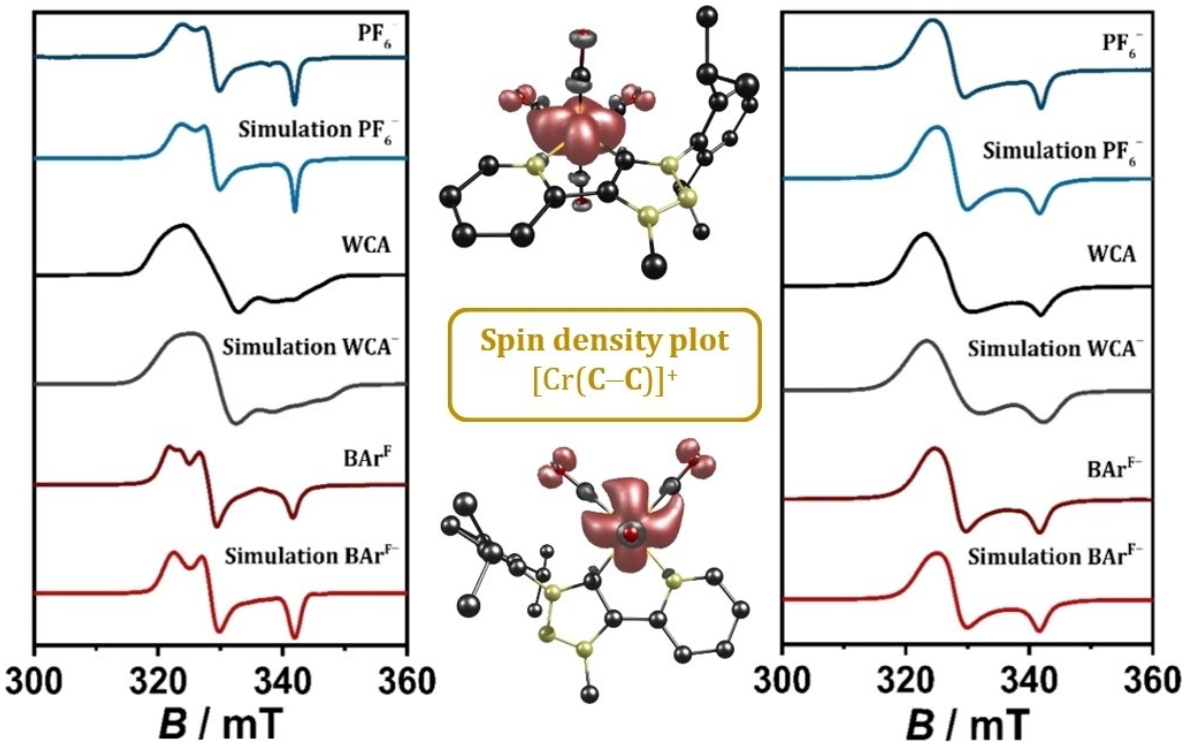

Figure 5. Left: EPR spectra of [Cr(C–C)](X). Right: EPR spectra of [Cr(C–N)](X). Electrochemically generated in 0.1 M NBu_4PF_6/CH_3CN at −175 °C (blue: PF_6^-, light blue: simulation) and chemically oxidized (X=WCA$^-$, BAr^{F-}) in CH_2Cl_2 at −175 °C (black: WCA$^-$, grey: simulation; dark red: BAr^{F-}, red: simulation). Center: Calculated spin density plot of $[Cr(C–C)]^+$ (B3LYP/D3/def2-TZVP, iso value = 0.033).

in the crystals triggered our interest to further investigate the influence of the counterion on properties of the oxidized $[Cr(CO)_4(pyridyl\text{-}MIC)]^+$ framework.

[Cr(C–C)](X) with more interacting anions $X = PF_6^-$, BAr^{F-}[1] show rhombic EPR signals at $g_x = 2.09$, $g_y = 2.06$ and $g_z = 1.98$ with a *g*-anisotropy, Δg of up to 0.08, typical for predominantly metal-centered electron spins, and a partially resolved hyperfine coupling to the ^{53}Cr nucleus ($I = 3/2$, natural abundance: 9.55%). In addition, spin density calculation on the oxidized complex display about 99% spin on the chromium center (Figure 5 and Table S14).

Replacing the counterion in $[Cr(C–C)]^+$ from $[PF_6]^-$ and $[BAr^F]^-$ with $[WCA]^-$ results in a pseudo-axial EPR spectrum with hyperfine-coupling to the pyridyl-*N*. (Table S15 and Figure 5, left). The effect can also be noticed in [Cr(C-N)](WCA). The axial signal shows *g*-values of $g_\perp = 2.08$ and $g_{||} = 1.98$ with an unresolved pyridyl-*N* hyperfine coupling, caused by the strong anisotropic line broadening. In contrast, the EPR spectra with $[PF_6]^-$ and $[BAr^F]^-$ counterion show no hyperfine coupling to the pyridyl-*N*. Instead a dominant metal-centered spin with *g*-values of $g_\perp = 2.08$ and $g_{||} = 1.98$ for $[Cr(C–N)](PF_6)$, and $g_\perp = 2.06$ and $g_{||} = 1.98$ for $[Cr(C\text{-}N)](BAr^F)$, respectively, are observed (Table S**16**). The data are in good agreement with the previously reported spin density calculation for $[Cr(C\text{-}N)]^+$ indicating a predominantly chromium-centered spin of $> 99\%$.[1]

The "level of innocence" of so-called weakly coordinating anions, such as $[PF_6]^-$ and $[BAr^F]^-$, compared to the well-established $[Al(OR^F)_4]^-$ ($R^F = C(CF_3)_3$) has been intensively studied[32] and classical WCAs are often not as "innocent" as perceived. This effect is indeed present here: It is reasonable to assume, that the cation-anion interactions for $[PF_6]^-$ and $[BAr^F]^-$ are stronger compared to their WCA counterparts. PF_6^- is a small anion and the partial negative charges on the F-atoms are high which will increase the propensity of H···F and C···F interactions with the ligand. The ability of $[BAr^F]^-$ to undergo such interactions will be much smaller compared to the hexafluorophosphate anion. However, $[BAr^F]^-$ can undergo additional π··· π interactions. Neither of these interactions are very likely with WCA. Thus, $[PF_6]^-$ and $[BAr^F]^-$ reduce the electron deficiency of the $[Cr(CO)_4(pyridyl\text{-}MIC)]^+$ fragment, while $[WCA]^-$ remains "innocent" and truly non-interacting also in an electronic sense.

Consequently, the pyridyl-MIC ligands show stronger contributions to compensate for the electron deficiency, as evident from the EPR spectra of [Cr(C–C)](WCA) and [Cr(C-N)](WCA). The stronger hyperfine coupling of pyridyl-*N* (100 MHz) in [Cr(C–C)](WCA), if compared to the hyperfine coupling of 30 Hz in [Cr(C–N)](WCA), underlines the strong influence of the two constitutional isomers and is in good agreement with the overall σ–donor strengths.

Conclusions

In summary, we present the first isolated, crystalline and crystallographically characterized chromium $[Cr(CO)_4]^+$ complexes with pyridyl-MIC ligands that are not only strong σ–donors, but also strong π–acceptors. The chemically oxidized complexes were investigated by IR- and EPR-spectroscopy and compared with their electrochemically-generated analogues, supported by theoretical calculations. The combination of TD-DFT with our (spectro–)electrochemical measurements reveals the unique properties of the pyridyl-MIC ligands upon oxidation of the chromium metal-center. The strong σ–donor properties of the MIC ligand can compensate for the electron deficiency of $[Cr(CO)_4]^+$, which usually undergoes CO dissociation due to the reduced π–backbonding to the CO ligands, while largely retaining its MLCT character.

While the use of the pyridyl-MIC ligands alone is enough for the in situ generation and characterization of the 17 VE cationic Cr-carbonyl complex, its isolation in the pure form and crystallization needs the additional help from WCAs. Intriguingly, the fine-tuning of the electronic structure is not determined exclusively by the two ligand isomers, but also to a limited extent by the Lewis acid-base interactions with the counterions. The "classical" WCAs produce stronger ionic interactions compared to the $[Al(OR^F)_4]^-$ ($R^F = C(CF_3)_3$) type WCA, which have a direct influence on the contribution of the pyridyl-MIC moieties to their electronic structure. These results are of fundamental interest for the understanding of the electrochemical, photochemical and in general geometric/electronic structures of group 6 carbonyl complexes, as the isolation of kinetically labile complexes is no longer limited by purely electron-donating ligands,[33] but can also be achieved with ligands that are good π–acceptors.

Experimental Section

General procedures, materials and instrumentation

Caution! *Compounds containing azides are potentially explosive. Although we never experienced any problems during synthesis or analysis, all compounds should be synthesized only in small quantities and handled with great care!* Unless otherwise noted, all reactions were carried out using standard Schlenk-line-techniques under an inert atmosphere of argon (Linde Argon 4.8, purity 99.998%) or in a glovebox (Glovebox Systemtechnik, GS095218). Commercially available chemicals were used without further purification. The solvents used for metal complex synthesis and catalysis were available from MBRAUN MB-SPS-800 solvent System and degassed by standard techniques prior to use. The identity and purity of compounds were established via ^1H and ^{13}C NMR spectroscopy, elemental analysis and mass spectrometry. Solvents for cyclic voltammetry and UV/vis- and EPR-spectroelectrochemical measurements were dried and distilled under argon and degassed by common techniques prior to use. Column chromatography was performed over silica 60 M (0.04–0.063 mm). ^1H and $^{13}C\{^1H\}$ NMR spectra were recorded on a JOEL ECZ 400R spectrometer at 19–22 °C. Chemical shifts are reported in ppm referenced to the residual solvent peaks.[34] The following abbreviations are used to represent the multiplicity of the signals: s (singlet), d (doublet), t (triplet), q (quartet), p (pentet), sept (septet). Mass spectrometry was performed on an Agilent 6210 ESI-TOF. Elemental analyses were performed with an Elementar Micro Cube elemental analyser.

X-ray Diffraction: X-ray data were collected on a BRUKER Smart AXS, BRUKER D8 Venture or Bruker Kappa Apex2duo system. Data were collected at 100(2) or 140(2) K, respectively, using graphite-monochromatic MoK_α radiation (λ_α =0.71073 Å) or CuK_α radiation (λ_α =1.54178 Å), respectively. The strategy for the data collection was evaluated by using the APEX2 or Smart software. The data were collected by standard "ω scan techniques" or "$\omega - \varphi$ scan techniques" and were scaled and reduced using APEX2, SAINT+, and SADABS software. The structures were solved by direct methods using SHELXL-97 or intrinsic phasing using SHELXL-2014/7 and refined by full matrix least-squares with SHELXL-2014/7, refining on F^2. Non-hydrogen atoms were refined anisotropically. If it is noted, bond length and angles were measured with Mercury, version 3.8.[35]

Deposition Number(s) 2075622 (for [Cr(C–C)]), 2216773 (for [Cr-(C–C)](BAr^F)) and 2173735 (for [Cr(C–N)](WCA)) contain(s) the supplementary crystallographic data for this paper. These data are provided free of charge by the joint Cambridge Crystallographic Data Centre and Fachinformationszentrum Karlsruhe Access Structures service.

Electrochemistry: Cyclic voltammograms were recorded with a PalmSens4 potentiostat or PAR VersaStat (Ametek), respectively, with a conventional three-electrode configuration consisting of a glassy carbon working electrode, a platinum auxiliary electrode, and a coiled silver wire as a pseudo reference electrode. The (decamethyl)ferrocene/(decamethyl)ferrocenium couple was used as internal reference. All measurements were performed at room temperature with a scan rate between 25 and 1000 mVs^{-1}. The experiments were carried out in absolute Acetonitrile containing 0.1 M Bu_4NPF_6 (Sigma Aldrich, ≥99.0%, electrochemical grade) as the supporting electrolyte.

Spectroelectrochemistry: UV/vis spectra were recorded with a J&M TIDAS spectrometer or an Avantes spectrometer consisting of a light source (AvaLight-DH–S-Bal), a UV/Vis detector (AvaSpec-ULS2048), and an NIR detector (AvaSpec-NIR256-TEC). UV/vis-spectroelectrochemical measurements were carried out in an optically transparent thin-layer electrochemical (OTTLE)[36] cell (CaF_2 windows) with a gold-mesh working electrode, a platinum-mesh counter electrode, and a silver-foil pseudo reference. EPR spectra at the X-band frequency (ca. 9.5 GHz) were obtained with a Magnettech MS-5000 benchtop EPR spectrometer equipped with a rectangular TE 102 cavity and a TC HO4 temperature controller. The measurements were carried out in synthetic quartz glass tubes. For EPR spectroelectrochemistry, a three-electrode setup was employed using two Teflon-coated platinum wires (0.005 in. bare and 0.008 in. coated) as the working and counter electrodes and a Teflon-coated silver wire (0.005 in. bare and 0.007 in coated) as the pseudo reference electrode. The low temperature EPR-spectra were performed at −175 °C. The experiments were carried out in absolute Acetonitrile containing 0.1 M Bu_4NPF_6 as the supporting electrolyte. The same solvents as for the CV measurements were used for each compound. All EPR spectra recorder under chemical oxidation conditions were carried out in dry CH_2Cl_2.

Calculations: The program package ORCA 4.1. was used for all DFT calculations.[37] Starting from the molecular structure obtained from X-ray diffraction geometry optimizations were carried out using the B3LYP[38,39] functional and no symmetry restrictions were imposed during the optimization. All calculations were performed with empirical Van der Waals correction (D3).[40] The restricted and unrestricted DFT methods were employed for closed and open shell molecules respectively unless stated otherwise. Convergence criteria were set to default for geometry-optimization (OPT), and tight for SCF calculations (TIGHTSCF). Triple-ζ-valence basis sets (def2-TZVP)[41] were employed for all atoms. Calculations were performed using resolution of the identity approximation[42] with matching auxiliary basis sets[43] for geometry optimizations and numerical frequency calculations and the RIJCOSX (combination of the resolution of the identity and chain of spheres algorithms) approximation for single point calculations using the B3LYP functional.[38,39] Low-lying excitation energies were calculated with time-dependent DFT (TD-DFT). Solvent effects were taken into account with the conductor-like polarizable continuum model, CPCM.[44] Spin densities were calculated according to the Mulliken population analysis.[45] The absence of imaginary frequency Spin densities, molecular orbitals and difference densities were visualized with the modified Chemcraft 1.8 program.[46] All molecular orbitals are illustrated with an iso value of 0.052. All calculated TD-DFT spectra are Gaussian broadened with a band width of 25 nm at half height.

Synthesis of [Cr(C–C)]: A suspension of $[Cr(CO)_6]$ (11.7 mg, 0.053 mmol) in 6 mL THF was stirred for 2 h under UV light. The CO overpressure was released at least 3 times during this period. To the yellow solution $[H(C–C)]BF_4$[47] (21.7 mg, 0.053 mmol) and an excess of NEt_3 (0.6 mL) were added. The mixture was refluxed with an equipped reflux condenser and a gas bubbler overnight. After cooling to room temperature, the solvent was evaporated, and the residue was dissolved in 20 mL CH_2Cl_2 and extracted three times with 20 mL H_2O. The organic phases were collected and dried over Na_2SO_4. The solvent was reduced, and the crude product was purified by column chromatography (SiO_2, 100% CH_2Cl_2). Analytically pure product was isolated after recrystallization from CH_2Cl_2 and *n*-hexane yielding red crystals (16.4 mg, 64%).

^{1}H NMR (401 MHz, CD_3CN) δ = 9.12 ppm (dt, J=5.5, 1.1 Hz, 1H), 7.98–7.90 ppm (m, 2H), 7.59–7.54 ppm (m, 1H), 7.41 ppm (d, ^3J= 7.8 Hz, 2H), 7.31–7.26 ppm (m, 1H), 4.42 ppm (s, 3H, CH_3), 2.67 ppm (hept, ^3J=6.6 Hz, 2H, R_3CH), 1.30 ppm (d, ^3J=6.8 Hz, 6H, CH_3), 1.10 ppm (d, ^3J=6.8 Hz, 6H, CH_3); HRMS (ESI): m/z calcd for $C_{24}H_{24}CrN_4O_4^+$: 484.1203 [*Cr(C–C)*]$^+$; found: 484.1230; IR (CH_2Cl_2) $\tilde{\nu}$ = 1998 (m) cm^{-1}, 1890 (s) cm^{-1}, 1873 (sh) cm^{-1}, 1822 (s) cm^{-1} (C=O); ^{13}C NMR (176 MHz, CD_2Cl_2) δ = 231.76 ppm, 229.13 ppm, 218.03 ppm, 204.28 ppm, 156.07 ppm, 151.01 ppm, 146.41 ppm, 144.36 ppm, 137.17 ppm, 136.02 ppm, 131.30 ppm, 124.27 ppm, 123.26 ppm, 119.56 ppm, 39.01 ppm, 29.15 ppm, 25.79 ppm, 22.81 ppm; elemental analysis calcd (%) for $C_{24}H_{24}CrN_4O_4$: C 59.50, H 4.99, N 11.56; found: C 59.16, H 5.11, N 11.16.

Synthesis of [Cr(C–C)](BAr^F): In a synthetic glovebox, **[Cr(C–C)]** (20.1 mg, 0.042 mmol) was dissolved in CH_2Cl_2 and ferrocenium-tetrakis(3,5-bis(trifluoromethyl)phenyl)borate (44.1 mg, 0.042 mmol) was added. The red mixture changed immediately to yellow and was stirred for additional three hours at room temperature under the exclusion of light. The resulting yellow mixture was filtered through a syringe filter, overlaid with *n*-hexane, and placed in the freezer at −40 °C for two weeks yielding 50 mg (89%, 0.037 mmol) of crystalline [Cr(C–C)](BAr^F) suitable for X-ray diffraction analysis. In the case of remaining ferrocenium-tetrakis(3,5-bis(trifluoromethyl) phenyl)borate, the yellow solution was decanted, overlaid with additional *n*-hexane and again placed in the −40 °C freezer.

^{19}F NMR (235 MHz, CD_2Cl_2) δ = 62.80 ppm (BArF); HRMS (ESI): m/z calcd for $C_{24}H_{24}CrN_4O_4^+$: 484.1203; found [*Cr(C–C)*]$^+$: 484.1238; IR (CH_2Cl_2) $\tilde{\nu}$ = 2088 (m) cm^{-1}, 2016 (s) cm^{-1}, 1991 (sh) cm^{-1}, 1975 (s) cm^{-1} (C=O).

Synthesis of [Cr(C–N)](WCA): In a synthetic glovebox, [Cr(C–N)][1] (25.2 mg, 0.052 mmol) was dissolved in CH_2Cl_2 and $[Ag(Al(OC(CF_3)_3)_4]$[15] (WCA = $[Al(OC(CF_3)_3)_4]^-$) (58.7 mg, 0.055 mmol) was added. The dark red mixture changed immediately to orange and was stirred for additional three hours at room temperature under the exclusion of light. The resulting orange mixture was

filtered through a syringe filter, overlaid with *n*-hexane, and placed in the freezer at −40 °C for two weeks yielding 69 mg (87 %, 0.048 mmol) of crystalline [Cr(C–N)](WCA) suitable for X-ray diffraction analysis. In the case of remaining $[Ag(Al(OC(CF_3)_3)_4]$, the orange solution was filtered again through a syringe filter and overlaid with additional *n*-hexane or the orange solid is again dissolved and filtered through a syringe filter, too.

^{19}F NMR (235 MHz, CD_2Cl_2) $\delta = 75.67$ ppm ($Al(OC(CF_3)_3)_4$); HRMS (ESI): m/z calcd for $C_{24}H_{24}CrN_4O_4^+$: 484.1203 [*Cr(C–C)*]$^+$; found: 484.1234; IR (CH_2Cl_2) $\tilde{\nu} = 2089$ (m) cm^{-1}, 2018 (s) cm^{-1}, 1996 (sh) cm^{-1}, 1975 (s) cm^{-1} (C≡O).

Supporting Information

Cyclic voltammetry, ^1H and ^{19}F NMR spectroscopy, IR-, UV/vis/NIR- and EPR-spectroelectrochemistry, single X-ray diffraction data, synthesis, (TD)DFT calculations.

Acknowledgements

We further thank B. Förtsch for elemental analyses and Dr. W. Frey (Institut für Organische Chemie) for collecting the X-ray data sets and the support by the state of Baden-Württemberg through bwHPC and the German Research Foundation (DFG) through grant no INST 40/575-1 FUGG (JUSTUS 2 cluster). We kindly acknowledge the German Science Foundation (DFG, Priority Program SPP 2102 "Light-controlled reactivity of metal complexes", SA 1840/7-1 and SA 1840/7-2) for financial support. Open Access funding enabled and organized by Projekt DEAL.

Conflict of Interests

The authors declare no conflict of interest.

Data Availability Statement

The data that support the findings of this study are available in the Supporting Information of this article.

Keywords: carbonyl ligands · chromium(I) · mesoionic carbenes · (spectro)electrochemistry · weakly coordinating anions

[1] T. Bens, P. Boden, P. Di Martino-Fumo, J. Beerhues, U. Albold, S. Sobottka, N. I. Neuman, M. Gerhards, B. Sarkar, *Inorg. Chem.* **2020**, *59*, 15504–15513.
[2] P. Boden, P. Di Martino-Fumo, T. Bens, S. Steiger, U. Albold, G. Niedner-Schatteburg, M. Gerhards, B. Sarkar, *Chem. Eur. J.* **2021**, *27*, 12959–12964.
[3] P. J. Boden, P. Di Martino-Fumo, T. Bens, S. T. Steiger, D. Marhöfer, G. Niedner-Schatteburg, B. Sarkar, *Chem. Eur. J.* **2022**, *28*, e202201038.
[4] M. L. Clark, K. A. Grice, C. E. Moore, A. L. Rheingold, C. P. Kubiak, *Chem. Sci.* **2014**, *5*, 1894–1900.
[5] I. R. Farrell, P. Matousek, A. Vlček, *J. Am. Chem. Soc.* **1999**, *121*, 5296–5301.
[6] F. Franco, C. Cometto, F. Sordello, C. Minero, L. Nencini, J. Fiedler, R. Gobetto, C. Nervi, *ChemElectroChem* **2015**, *2*, 1372–1379.
[7] M. Isegawa, *Chem. Phys.* **2023**, *565*, 111758.
[8] D. Sieh, D. C. Lacy, J. C. Peters, C. P. Kubiak, *Chem. Eur. J.* **2015**, *21*, 8497–8503.
[9] M. Tang, L. Cameron, E. M. Poland, L.-J. Yu, S. A. Moggach, R. O. Fuller, H. Huang, J. Sun, S. C. Thickett, M. Massi, M. L. Coote, C. C. Ho, A. C. Bissember, *Inorg. Chem.* **2022**, *61*, 1888–1898.
[10] J. Tory, B. Setterfield-Price, R. A. W. Dryfe, F. Hartl, *ChemElectroChem* **2015**, *2*, 213–217.
[11] A. Vlček Jr., *Coord. Chem. Rev.* **2002**, *230*, 225–242.
[12] a) T. Scherpf, C. R. Carr, L. J. Donnelly, Z. S. Dubrawski, B. S. Gelfand, W. E. Piers, *Inorg. Chem.* **2022**, *61*, 13644–13656; b) J. Agarwal, T. W. Shaw, C. J. Stanton, G. F. Majetich, A. B. Bocarsly, H. F. Schaefer, *Angew. Chem. Int. Ed. Engl.* **2014**, *53*, 5152–5155; c) E. E. Benson, C. P. Kubiak, *Chem. Commun.* **2012**, *48*, 7374–7376; d) V. Blaszczak, M. McKinnon, L. Suntrup, N. A. Aminudin, B. Reed, S. Groysman, M. Z. Ertem, D. C. Grills, J. Rochford, *Inorg. Chem.* **2022**, *61*, 15784–15800; e) M. Bourrez, F. Molton, S. Chardon-Noblat, A. Deronzier, *Angew. Chem. Int. Ed. Engl.* **2011**, *50*, 9903–9906; f) F. Franco, M. F. Pinto, B. Royo, J. Lloret-Fillol, *Angew. Chem. Int. Ed. Engl.* **2018**, *57*, 4603–4606; g) K. A. Grice, N. X. Gu, M. D. Sampson, C. P. Kubiak, *Dalton Trans.* **2013**, *42*, 8498–8503; h) J. Hawecker, J.-M. Lehn, R. Ziessel, *J. Chem. Soc. Chem. Commun.* **1984**, 328–330; i) J. A. Keith, K. A. Grice, C. P. Kubiak, E. A. Carter, *J. Am. Chem. Soc.* **2013**, *135*, 15823–15829; j) C. W. Machan, M. D. Sampson, S. A. Chabolla, T. Dang, C. P. Kubiak, *Organometallics* **2014**, *33*, 4550–4559; k) J. F. Martinez, N. T. La Porte, S. Chaudhuri, A. Sinopoli, Y. J. Bae, M. Sohail, V. S. Batista, M. R. Wasielewski, *J. Phys. Chem. C* **2019**, *123*, 10178–10190; l) T. Scherpf, C. Carr, L. Donnelley, Z. Dubrawski, W. Piers, B. Gelfand, *ChemRxiv.* **2022**; m) H. Shirley, T. M. Sexton, N. P. Liyanage, C. Z. Palmer, L. E. McNamara, N. I. Hammer, G. S. Tschumper, J. H. Delcamp, *Eur. J. Inorg. Chem.* **2020**, *2020*, 1844–1851; n) J. M. Smieja, M. D. Sampson, K. A. Grice, E. E. Benson, J. D. Froehlich, C. P. Kubiak, *Inorg. Chem.* **2013**, *52*, 2484–2491; o) B. P. Sullivan, C. M. Bolinger, D. Conrad, W. J. Vining, T. J. Meyer, *J. Chem. Soc. Chem. Commun.* **1985**, 1414–1416; p) L. Suntrup, F. Stein, J. Klein, A. Wilting, F. G. L. Parlane, C. M. Brown, J. Fiedler, C. P. Berlinguette, I. Siewert, B. Sarkar, *Inorg. Chem.* **2020**, *59*, 4215–4227.
[13] a) P. Datta, D. Sardar, A. P. Mukhopadhyay, E. López-Torres, C. J. Pastor, C. Sinha, *J. Organomet. Chem.* **2011**, *696*, 488–495; b) D. M. Manuta, A. J. Lees, *Inorg. Chem.* **1986**, *25*, 1354–1359; c) S. Zális, I. R. Farrell, A. Vlcek, *J. Am. Chem. Soc.* **2003**, *125*, 4580–4592.
[14] F. Ma, M. Jarenmark, S. Hedström, P. Persson, E. Nordlander, A. Yartsev, *RSC Adv.* **2016**, *6*, 20507–20515.
[15] a) A. M. Bond, R. Colton, J. E. Kevekordes, P. Panagiotidou, *Inorg. Chem.* **1987**, *1987*, 1430–1435; b) S. Ernst, W. Kaim, *Inorg. Chim. Acta* **1986**, *114*, 123–125.
[16] A. M. Bond, R. Colton, J. E. Kevekordes, P. Panagiotidou, *Inorg. Chem.* **1987**, *26*, 1430–1435.
[17] S. Ernst, W. Kaim, *J. Am. Chem. Soc.* **1986**, *108*, 3578–3586.
[18] I. R. Farrell, F. Hartl, S. Záliš, M. Wanner, W. Kaim, A. Vlček, *Inorg. Chim. Acta* **2001**, *318*, 143–151.
[19] J. Hanzlík, L. Pospíšil, A. A. Vlček, M. Krejčík, *J. Electroanal. Chem.* **1992**, *331*, 831–844.
[20] R. Johnson, H. Madhani, J. P. Bullock, *Inorg. Chim. Acta* **2007**, *360*, 3414–3423.
[21] a) I. R. Farrell, J. van Slageren, S. Záliš, A. Vlček, *Inorg. Chim. Acta* **2001**, *315*, 44–52; b) K. A. Rawlins, A. J. Lees, *Inorg. Chem.* **1989**, *28*, 2154–2160; c) P. C. Servaas, H. K. van Dijk, T. L. Snoeck, D. J. Stufkens, A. Oskam, *Inorg. Chem.* **1985**, *24*, 4494–4498; d) D. J. Stufkens, *Coord. Chem. Rev.* **1990**, *104*, 39–112.
[22] D. M. Manuta, A. J. Lees, *Inorg. Chem.* **1986**, *25*, 1354–1359.
[23] R. W. Balk, T. Snoeck, D. J. Stufkens, A. Oskam, *Inorg. Chem.* **1980**, *19*, 3015–3021.
[24] a) R. S. Panesar, N. Dunwoody, A. J. Lees, *Inorg. Chem.* **1998**, *37*, 1648–1650; b) S. Wieland, K. B. Reddy, R. van Eldik, *Organometallics* **1990**, *9*, 1802–1806.
[25] D. Miholová, B. Gaš, S. Záliš, J. Klíma, A. A. Vlček, *J. Organomet. Chem.* **1987**, *330*, 75–84.
[26] L. Suntrup, S. Klenk, J. Klein, S. Sobottka, B. Sarkar, *Inorg. Chem.* **2017**, *56*, 5771–5783.
[27] a) G. Guisado-Barrios, M. Soleilhavoup, G. Bertrand, *Acc. Chem. Res.* **2018**, *51*, 3236–3244; b) R. Maity, B. Sarkar, *JACS Au* **2022**, *2*, 22–57; c) K. O. Marichev, S. A. Patil, A. Bugarin, *Tetrahedron* **2018**, *74*, 2523–

2546; d) Á. Vivancos, C. Segarra, M. Albrecht, *Chem. Rev.* **2018**, *118*, 9493–9586.
[28] a) J. Bohnenberger, W. Feuerstein, D. Himmel, M. Daub, F. Breher, I. Krossing, *Nat. Commun.* **2019**, *10*, 1–8; b) J. Bohnenberger, D. Kratzert, S. M. N. V. T. Gorantla, S. Pan, G. Frenking, I. Krossing, *Chem. Eur. J.* **2020**, *26*, 17203–17211; c) J. Bohnenberger, I. Krossing, *Angew. Chem. Int. Ed. Engl.* **2020**, *59*, 5581–5585; d) J. Bohnenberger, M. Schmitt, W. Feuerstein, I. Krummenacher, B. Butschke, J. Czajka, P. J. Malinowski, F. Breher, I. Krossing, *Chem. Sci.* **2020**, *11*, 3592–3603; e) J. M. Rall, M. Schorpp, M. Keilwerth, M. Mayländer, C. Friedmann, M. Daub, S. Richert, K. Meyer, I. Krossing, *Angew. Chem. Int. Ed. Engl.* **2022**, *61*, e202204080; f) M. Schmitt, M. Mayländer, J. Goost, S. Richert, I. Krossing, *Angew. Chem. Int. Ed. Engl.* **2021**, *60*, 14800–14805; g) W. Unkrig, M. Schmitt, D. Kratzert, D. Himmel, I. Krossing, *Nat. Chem.* **2020**, *12*, 647–653.
[29] N. G. Connelly, W. E. Geiger, *Chem. Rev.* **1996**, *96*, 877–910.
[30] I. Krossing, *Chem. Eur. J.* **2001**, *7*, 490–502.
[31] L. E. Bowen, M. F. Haddow, A. G. Orpen, D. F. Wass, *Dalton Trans.* **2007**, 1160–1168.
[32] I. M. Riddlestone, A. Kraft, J. Schaefer, I. Krossing, *Angew. Chem. Int. Ed. Engl.* **2018**, *57*, 13982–14024.
[33] A. J. Rucklidge, D. S. McGuinness, R. P. Tooze, A. M. Z. Slawin, J. D. A. Pelletier, M. J. Hanton, P. B. Webb, *Organometallics* **2007**, *26*, 2782–2787.
[34] S. Budavari (Ed.) *The MERCK Index. An Encyclopedia of Chemical, Drugs and Biologicals*, Merck & Co, Rahway, **1989**.
[35] a) APEX3. v2015.5-2, Bruker AXS Inc, Madison, Wisconsin (USA), **2015**; b) G. M. Sheldrick, SHELXS-97 and SHELXL-97, Program for Crystal Structure Solution and Refinement, University of Gottingen, Göttingen (Germany), **1997**; c) G. M. Sheldrick, Program for Empirical Absorption Correction. SADABS Version 2008/1, University of Göttingen, Göttingen (Germany), **2008**; d) G. M. Sheldrick, Program for Crystal Structure Solution and Refinement. SHELXL Version 2014/7, University of Göttingen, Göttingen (Germany), **2014**; e) C. F. Macrae, P. R. Edgington, P. McCabe, E. Pidcock, G. P. Shields, R. Taylor, M. Towler, J. van de Streek, *J. Appl. Crystallogr.* **2006**, *39*, 453–457; f) SAINT+, Data Integration Engine. Version 8.27b ©, Bruker AXS Inc., Madison, Wisconsin (USA), 1997–2012; g) G. M. Sheldrick, *Acta Crystallogr.* **2008**, *A64*, 112–122; h) G. M. Sheldrick, *Acta Crystallogr.* **2015**, *C71*, 3–8.
[36] a) J. Klein, A. Stuckmann, S. Sobottka, L. Suntrup, M. van der Meer, P. Hommes, H.-U. Reissig, B. Sarkar, *Chem. Eur. J.* **2017**, *23*, 12314–12325; b) M. Krejčik, M. Daněk, F. Hartl, *J. Electroanal. Chem. Interfacial Electrochem.* **1991**, *317*, 179–187.
[37] F. Neese, *WIREs Comput. Mol. Sci.* **2012**, *2*, 73–78.
[38] A. D. Becke, *J. Chem. Phys.* **1993**, *98*, 5648–5652.
[39] C. Lee, W. Yang, R. G. Parr, *Phys. Rev. B* **1988**, *37*, 785–789.
[40] a) S. Grimme, *J. Comput. Chem.* **2004**, *25*, 1463–1473; b) S. Grimme, *J. Comput. Chem.* **2006**, *27*, 1787–1799; c) S. Grimme, J. Antony, S. Ehrlich, H. Krieg, *J. Chem. Phys.* **2010**, *132*, 154104; d) S. Grimme, S. Ehrlich, L. Goerigk, *J. Comput. Chem.* **2011**, *32*, 1456–1465.
[41] F. Weigend, R. Ahlrichs, *Phys. Chem. Chem. Phys.* **2005**, *7*, 3297–3305.
[42] a) R. Izsák, F. Neese, *J. Chem. Phys.* **2011**, *135*, 144105–1-144105-11; b) F. Neese, *J. Comput. Chem.* **2003**, *24*, 1740–1747; c) F. Neese, G. Olbrich, *Chem. Phys. Lett.* **2002**, *362*, 170–178; d) F. Neese, F. Wennmohs, A. Hansen, U. Becker, *Chem. Phys.* **2009**, *356*, 98–109; e) T. Petrenko, S. Kossmann, F. Neese, *J. Chem. Phys.* **2011**, *134*, 054116–1-054116-14; f) O. Vahtras, J. Almlöf, M. W. Feyereisen, *Chem. Phys. Lett.* **1993**, *213*, 514–518; g) J. L. Whitten, *J. Chem. Phys.* **1973**, *58*, 4496–4501.
[43] a) K. Eichkorn, O. Treutler, H. Öhm, M. Häser, R. Ahlrichs, *Chem. Phys. Lett.* **1995**, *242*, 652–660; b) K. Eichkorn, F. Weigend, O. Treutler, R. Ahlrichs, *Theor. Chem. Acc.* **1997**, *97*, 119–124.
[44] V. Barone, M. Cossi, *J. Phys. Chem. A* **1998**, *102*, 1995–2001.
[45] R. S. Mulliken, *J. Chem. Phys.* **1955**, *23*, 1833–1840.
[46] G. A. Zhurko, Chemcraft-Graphical Program for Visualization of Quantum Chemistry Computations. Ver. 1.8., http://www.chemcraftprog.com/, Ivanovo (Russia), **2023**.
[47] T. Bens, J. A. Kübler, R. R. M. Walter, J. Beerhues, O. S. Wenger, B. Sarkar, *ACS Org. Inorg. Au* **2023**, https://doi.org/10.1021/acsorginorgau.3c00005.

Manuscript received: April 17, 2023
Accepted manuscript online: May 22, 2023
Version of record online: July 17, 2023